This is the peer-reviewed, final accepted version for American Mineralogist, published by the Mineralogical Society of America.
The published version is subject to change. Cite as Authors (Year) Title. American Mineralogist, in press.
DOI: https://doi.org/10.2138/am-2021-7563. http://www.minsocam.org/

Revision 2

ARTICLE

Stöfflerite, $(Ca,Na)(Si,Al)_4O_8$ in the hollandite structure: A new high-pressure polymorph of anorthite from martian meteorite NWA 856

OLIVER TSCHAUNER[1], CHI MA[2], JOHN G. SPRAY[3], ERAN GREENBERG[4], AND VITALI B. PRAKAPENKA[4]

[1]Department of Geoscience, University of Nevada Las Vegas, NV 89154, USA

[2]Division of Geological and Planetary Sciences, California Institute of Technology, Pasadena, CA 91125, USA

[3]Planetary and Space Science Centre, University of New Brunswick, NB E3B 5A3, Canada

[4]GSECARS, University of Chicago, Argonne National Laboratory, Lemont, IL 60439, USA

ABSTRACT

We present the crystal structure, composition and occurrence of stöfflerite, the naturally occurring Ca-aluminosilicate with hollandite-type structure. Stöfflerite is a high-pressure polymorph of anorthite and an approved mineral. The type material was found in the shergottitic martian meteorite Northwest Africa 856. Type stöfflerite ($Sto_{60}Lin_{40}$) assumes space group *I*4/*m* with unit cell dimensions a = 9.255(1) Å, c = 2.742(3) Å, V = 235.1(2) Å^3, and Z = 2.

INTRODUCTION

Feldspars are rock-forming minerals in planetary crusts. The feldspar endmembers albite, orthoclase, and anorthite have high-pressure polymorphs that assume the hollandite-type structure (Ringwood et al. 1967; Liu 1978; Gautron and Madon 1994). In this tetragonal

structure, Al and Si are six-fold coordinated by O within distorted octahedra. Edge-sharing $(Si,Al)O_6$-octahedra form double chains along the c-axis and the double chains are arranged to form channels through joined corners of the octahedra. Na, K, and Ca reside in these channels. The structure type is derived from the isotypic manganate hollandite KMn_4O_8, which itself is related to the rutile structure (Bystrøm and Bystrøm 1950; Post and Burnham 1986; Anderson and Hyde 1989). $NaAlSi_3O_8$-hollandite and $KAlSi_3O_8$-hollandite have been reported previously as minerals with the names lingunite (Gillet et al. 2001) and liebermannite (Ma et al. 2018), respectively. Recently, liebermannite was detected as a terrestrial mineral in a dianond inclusion (Huang et al. 2020). Here we report the natural occurrence of $(Ca,Na)(Si,Al)_4O_8$-hollandite, which has recently been approved as a mineral (IMA 2017-062; Tschauner and Ma 2017). The name stöfflerite is in honour of Dieter Stöffler, former director of the Museum für Naturkunde, Berlin, for his contributions to the field of shock metamorphism in meteorites and terrestrial impact structures.

Prior to full structural characterization and approval as a mineral, observation of $(Ca,Na)(Si,Al)_4O_8$-hollandite was reported by Langenhorst and Poirier (2000) via transmission electron microscopy and by Beck et al. (2004) via Raman-spectroscopy from a shock melt pocket in the Zagami shergottite, and by Spray & Boonsue (2016) and Boonsue & Spray (2017) from the Manicouagan impact structure, Canada, based on electron backscatter diffraction (EBSD) and Raman spectroscopy. Unlike liebermannite, the endmembers lingunite and stöfflerite do not appear to have thermodynamic stability fields. Above 14 GPa, anorthite decomposes into grossular, kyanite, and corundum (Liu 1978; Liu et al. 2012). This assemblage transforms above 20 GPa into zagamiite, $CaSiO_3$-perovskite, and stishovite along a negative, and above 22 to >28 GPa into $CaSiO_3$-perovskite, corundum, and stishovite along a markedly

positive Clapeyron-slope (Akaogi et al. 2009; Liu et al. 2012). $CaAl_2Si_2O_8$-hollandite has been reported from a laser-heating experiment on anorthite in diamond anvil cells above 14 GPa (Gautron and Madon 1994), but not in an earlier similar experiment by Liu (1978). Synthesis of $CaAl_2Si_2O_8$-hollandite was not reproduced by Liu et al. (2012) and Kubo et al. (2017). Stöfflerite is expected to occur as a minor component in liebermannite in possible alkaline-rich rock in the mantle transition zone. As a free phase the occurrence of stöfflerite is limited to shock metamorphic environments with dynamic pressures exceeding 20 GPa at temperatures sufficient to transform shock-compressed Ca-rich plagioclase into the dense crystalline structure of stöfflerite. This is below temperatures that allow the formation of the equilibrium phases zagamiite plus stishovite (see Implications and Beck et al. 2004). Stöfflerite and the clinopyroxene tissintite (Ma et al. 2015) are the only high-pressure polymorphs of Ca-rich plagioclase reported from nature.

EXPERIMENTAL METHODS

The holotype of stöfflerite is in a polished thin section of NWA (Northwest Africa) 856, which belongs to E. Stolper's Martian Meteorite Collection of the Division of Geological and Planetary Sciences, California Institute of Technology, Pasadena, California 91125, USA. Sample imagery was acquired using a ZEISS 1550 VP Field Emission Scanning Electron Microscope at Caltech, operated at 15 or 10 kV and a beam current of 2-4 nA. The electron backscatter diffraction (EBSD) analysis was attempted using an HKL EBSD system on the ZEISS 1550VP SEM. Quantitative wavelength-dispersive elemental microanalysis of the type material was performed using a JEOL 8200 electron microprobe operated at 10 kV and 5 nA in focused beam mode with a probe diameter of ~120 nm at Caltech. Analyses were processed with

the CITZAF correction procedure. Standards, number of analyses, range, 1-σ standard deviation, and composition of type material are given in Table 1.

Synchrotron diffraction data were obtained at the GSECARS undulator beamline 13-IDD, Advanced Photo Source, Argonne National Laboratory, USA, using a microfocused beam (3×4 μm²) of λ = 0.4133 Å and a MAR165 CCD area detector. Sample detector distance and geometric correction factors were determined using GSE-ADA (Dera et al. 2013) and Dioptas (Prescher and Prakapenka 2015). Integration of diffraction frames was conducted with Dioptas software. Diffraction data cover a range down to ~0.69 Å.

OCCURRENCE

The shergottitic meteorite NWA 856 consists mainly of high- and low-Ca pyroxene (augite and pigeonite) and maskelynite, with accessory ilmenite, titanomagnetite, chromite, baddeleyite, merrillite, apatite, and pyrrhotite. Shock melt pockets (up to 0.5 cm diameter) occur scattered throughout the meteorite. High-pressure metamorphic phases occur within, or in proximity to, the melt pockets include stishovite and zagamiite (Beck et al. 2004; Ma et al. 2017, 2019). Shock melt pockets are the result of 'hot spot' formation during shock compression via the collapse of voids, exothermic chemical reactions, or large local contrasts in shock-impedance generate locally high temperatures. In shocked meteorites, as well as in terrestrial impactites, high pressure minerals are commonly observed only within or around such hot spots or shock-melt veins where high temperatures allow for overcoming kinetic barriers of stress-induced structural transitions and reactions over the duration of the state of shock compression (see, for instance, Sharp and de Carli 2006), whereas the minerals in the bulk of the rock experience extreme deformation or, in case of some minerals, pressure-induced vitrification, but are not

transformed to high-pressure polymorphs (Stöffler et al. 2018). Thus, occurrences of high-pressure minerals are limited to small regions within the shocked meteorites and even within these regions, paragenesis varies on the scale of few micrometers along the commonly steep temperature gradient (see, for example, Biren & Spray 2011; Walton et al. 2014, Ma et al. 2016). Here we used high-resolution FE-SEM, electron probe microanalysis (EPMA), and synchrotron X-ray diffraction (SXRD) to characterize the composition and structure of $(Ca,Na)(Si,Al)_4O_8$ in the hollandite form. This phase vitrifies with volume expansion under the electron beam (Fig. 1); therefore electron backscatter diffraction (EBSD) analysis failed to reveal any diffraction pattern. The mineral occurs as fine-grained crystalline masses in regions between diaplectic plagioclase (maskelynite) and the actual melt pocket (Fig. 1). The average grain size of stöfflerite is estimated as 20±5 nm based on the Scherrer equation of SXRD analysis. The occurrence of stöfflerite is noticeable in BSE imagery by a phase contrast with adjacent maskelynite of equal composition, and by a pronounced beam-sensitivity (Fig. 1). Stöfflerite occurs in association with zagamiite and stishovite (Fig. 1). In accordance with previous experimental studies on a more sodic and potassic feldspathic bulk composition (Tomioka et al. 2000), and on the Mg-bearing CAS system (Madon et al. 1989), the paragenesis is consistent with a transformation sequence: diaplectic glass → stöfflerite → zagamiite + stishovite along the temperature gradient of the shock-melt pocket and its surroundings.

Stöfflerite is colorless and transparent. Lustre, streak, hardness, tenacity, cleavage, fracture, density, and optical properties could not be determined because of the small grain size of the type material. Synthetic material of this composition is currently not available. Analytical results are given in Table 1. The EPMA data indicate that the maskelynite is of intermediate composition (average An_{60}). The empirical formula of the type stöfflerite (based on 8 O atoms

pfu) is $(Ca_{0.55}Na_{0.36}K_{0.02})(Al_{1.49}Fe_{0.03})Si_{2.49}O_8$, which suggests vacancies on site 2b. However, the diffraction data analysis does not indicate such a deficit within uncertainties. We assign this difference to migration of Na out of the electron beam during analysis. The general formula is $(Ca,Na)(Si,Al)_4O_8$. The endmember formula is $CaAl_2Si_2O_8$.

RESULTS

Diffraction patterns of stöfflerite are powder-like with smooth Debye fringes. The patterns were identified immediately by their similarity to the calculated diffraction pattern of liebermannite. Zagamiite and a minor amount of stishovite contribute to the patterns. We selected a pattern where stöfflerite is the dominant phase by >80 vol. % (Fig. 2) and refined the unit cell, site occupancies, and fractional atomic coordinates using the Rietveld method. In addition, we conducted a Le Bail extraction of apparent |F(hkl)|. We used this set of structure factor moduli for a global optimization without symmetry bias (i.e., in space group *P*1) using a reversed Monte Carlo approach (Putz et al. 1999). In this method, an extensive range of the configuration space is sampled with assumptions about neither symmetry nor structure of the phase. The global optimization converged with an R_F of 0.16. An automatic symmetry search after convergence of the global optimization resulted in space group *I*4/*m* and the hollandite structure. The recovery of the hollandite structure through global optimization shows that the structure model is correct.

Rietveld refinement was conducted with Powdercell (Kraus and Nolze 1996) and with GSAS (Larson and von Dreele 2004) and converged in both cases to $R_{wp} = 0.15$ and $R_p = 0.09$ for 3367 observations with a reduced χ^2 of 5.35. The Le Bail extraction converged to an $R_{wp} = 0.14$ and the R_F was 0.16. The values of the converged refinement parameters are somewhat affected by a modulated background that is generated by instrumental diffuse scattering in the

beamline hutch. However, we found the refined fractional atomic coordinates and site-occupancies to be unaffected by different background treatment in GSAS and Powdercell within the given uncertainties. The pattern of stöfflerite is pronounced and the identification of this phase through powder X-ray diffraction is unambiguous (Fig 2). For refinement of the site occupancies we used the Ca- and K-content from EPMA, but allowed the Na content to vary in order to examine a possible partial occupancy of site 2b. However, within uncertainties, site 2b is fully occupied. We repeated refinement starting with much more sodic or calcic trial compositions and used the fully converged results for assessment of uncertainties (see deposited cif). The sum of Si + Al was fixed by charge balance. Stöfflerite is tetragonal in space group $I4/m$, with unit cell dimensions a = 9.255(1) Å, c = 2.742(3) Å, V = 234.9(3) Å^3, and Z = 2. The calculated density is 3.84(1) g/cm^3 using the empirical formula.

IMPLICATIONS

Since this paper reports the first structure analysis of $(Ca,Na)(Si,Al)_4O_8$ in the hollandite structure, it is worthwhile examining the three hollandite-type polymorphs of the feldspars in comparison. As already noted by Ringwood et al. (1967), in the silicate-hollandites, the c-axis length corresponds directly to the O1-O1 and O2-O2 interatomic distances along 001. This relation holds also for stöfflerite: c-axis length and O-O distances along 001 are both 2.743 Å. In liebermannite and lingunite, the equivalent distances are 2.706 and 2.746 Å, respectively (Zhang et al. 1993, Liu 1978). In stöfflerite, no indication for site ordering has been found: Site ordering requires a structural transformation, for instance to subgroup $I2/m$ (space group No. 12 in the 15th setting) where the cation site remains single and general but the (Si,Al)- and the O-sites each split into two distinct sites. The central cation would be surrounded by alternating double-chains

of aluminate- and silicate octahedra. Alternation of aluminate and silicate along the chains implies further symmetry-reduction at least through formation of a supercell. We found no indication for a monoclinic distortion of the unit cell or for superlattice reflections. Ordering of Na and Ca along the channels and within the tetragonal metric implies marked changes in |F(hkl)|s or formation of a supercell. None of this is observed or resolved. It has been noted earlier (Zhang et al. 1993, Post and Burnham 1986) that hollandite-type structures do not exhibit ordering of the cations or charges in the octahedral sites. Generally, and in contrast to alumosilicates with tetrahedral framework structures, the more extended Si-O and Al-O bond distances in high-pressure phases with octahedrally coordinated Si and Al appear to release the sterical constraints that impose the Loewenstein rule (Loewenstein 1954). Si-Al site disorder in high-pressure phases with $Al^{[6]}$- and $Si^{[6]}$-O polyhedra has been confirmed for a number of cases including liebermannite (Zhang et al. 1993), zagamiite (Ma et al. 2019), the NAL-phase (Pamato et al. 2014), and a structurally related K-rich phase (Gasparik et al. 2000). Bond distances in the stöfflerite structure can be computed based on the deposited cif and compared to those of liebermannite and lingunite (Zhang et al. 1993; Liu 1978). In stöfflerite, liebermannite, and lingunite, the (Si,Al)-O bond distances are noticeably unequal with ratios of 1.06, 1.05, 1.05, respectively, whereas in stishovite the Si-O bond length ratio is 1.03 (Kirfel et al. 2001). The elongated (Si,Al)-O1 bond distance in the silicate-hollandites corresponds to a (Ca,K,Na)-O1 distance shorter than the other (Ca,K,Na)-O distances. It is plausible that this distortion of the octahedral units compensates for sterical constraints and thereby lifts crystal-chemical constraints like the Loewenstein-rule. In silicate-hollandites, compressibility is mostly controlled by the octahedral framework (Zhang et al. 1993). The narrow stability field of liebermannite and the absence of any stability field of stöfflerite and lingunite (at least at high Na-content) suggests

that this framework is not sufficiently flexible to compensate extensive compression, imposed either by external pressure or chemical substitution, through tilt and distortion of the octahedral units.

As mentioned in the introduction, stöfflerite does not have a thermodynamic stability field. In alkaline rocks in the Earth's mantle (such as in subducted slabs), it is expected to occur only as minor component in solid solution with liebermannite. Liebermannite with a minor component of stöfflerite has been reported in an experimental study by Greaux et al. (2017) on KREEP-like rock above 14 GPa. Recently, evidence for the existence of liebermannite in a diamond-inclusion from the Earth's transition zone was reported by Huang et al. (2020). This natural liebermannite from the Earth's mantle contains ~5 mol% lingunite but no stöfflerite component beyond uncertainty. The relevance of stöfflerite as a free phase is in its occurrence as an intermediate phase around hotspots within shocked feldspar-rich rock. Along the temperature gradient of the hotspot (Fig. 1), we observe in NWA 856 and in Zagami the sequence diaplectic glass → stöfflerite → zagamiite + stishovite. We first discuss this paragenesis with respect to the thermodynamic phase diagram, then discuss the issue of kinetic barriers, which are essential in understanding formation of a metastable mineral like stöfflerite.

The paragenesis zagamiite + stishovite is consistent with the thermodynamic phase diagram of the CAS system with anorthite bulk composition between 20 and 22 GPa (Liu et al. 2012). Under these conditions the stable assemblage is zagamiite + stishovite + $CaSiO_3$-perovskite and is replaced by corundum + stishovite + $CaSiO_3$-perovskite above 22 to 26 GPa along a strongly positive Clapeyron-slope (Akaogi et al. 2009), while at pressures between 12 and 20 GPa zagamiite occurs together with grossular-rich garnet and kyanite (Liu et al. 2012). In comparing the paragenesis in the shock melt pockets in plagioclase grains of NWA 856 and

Zagami with the stable paragenesis at 20-22 GPa, it is assumed that $CaSiO_3$-perovskite was present in the shock melt pockets but has vitrified upon release and does not generate distinct X-ray diffraction or EBSD patterns. Other than $CaSiO_3$-perovskite, corundum and grossular can be conserved upon shock-release and should be observable if they have formed.

Thermodynamic phase boundaries and kinetic boundaries in dynamically compressed materials are generally not equal. Also, phases may have formed upon crystallization of melt upon release from the shock state. Langenhorst and Poirier (2000) argue that silicate-hollandites in shock-melt veins from Zagami have formed through crystallization from melt upon release while the peak shock pressure was between 25- 30 GPa. This estimate is based on deformation features in bulk rock minerals and has been further narrowed by Fritz et al. (2005) to be 29.5 ± 0.5 GPa. However, Langenhorst and Poirier (2000) based their interpretation on earlier experimental studies, which suggested that silicate-hollandites are solidus phases in the CAS phase diagram. Later this assumption has been shown to be incorrect in a number of studies (e.g., Akaogi et al. 2009; Akaogi et al. 2010; Liu et al. 2012). Growth of metastable phases from dynamically compressed melts is perceivable. However, to our knowledge such metastable crystallization has not been observed in shock-melt pockets of shergottites. Beck et al. (2004) noticed the mismatch between peak shock pressures based on deformation features and the stability field of the high-pressure phases in the CAS phase diagram. They proposed local stress excursion as a plausible explanation of this difference.

Ma et al. (2016) found no marked difference between static and dynamic boundaries of high-pressure phases at the rim shock-melt pockets in the Tissint shergottite, where bridgmanite-wüstite intergrowths were observed. Because of the very steep rise of solidus temperatures in the MFS system at pressures of bridgmanite stability, a significant overriding of thermodynamic

boundaries would result in rather high release temperatures at low pressures and bridgmanite would not be conserved as a crystalline phase (Tschauner et al. 2014). If this agreement also holds for Zagami and NWA 856, the peak shock pressures for these meteorites are 20-22 GPa rather than 29-30 GPa. Similar differences have been reported for chondrites (Sharp and DeCarli 2006). However, in absence of a phase like bridgmanite, which provides a strong constraint on the peak- and release temperatures, the question whether there is a systematic offset in assessments or a real difference in dynamic stress regimes of bulk rock and hot spots have to be left open for NWA 856 and Zagami. We note that shock-induced formation of melts induces a local reduction in dynamic stress, at least over a particular time interval. In principle, this stress-temperature correlation, as well as its temporal evolution, are assessable through the ZND theory (e.g. Zel'dovich & Raizer, 2002). This computation, however, requires better knowledge of caloric and thermoelastic parameters of the involved phases than currently available.

The comparison between Tissint and NWA 856 is interesting with respect to the metastable formation of stöfflerite. In Tissint, the stable phase assembly bridgmanite + wüstite is observed at the rim of the melt pockets but at distances of 5-100 μm away from the border, Ma et al. (2016) observed ahrensite and ringwoodite as metastable high-pressure phases that clearly have formed far beyond their stability fields. Their formation was explained by the kinetic boundaries along the temperature gradient: At distances of a few to several micrometers, the dynamic temperature was sufficient to convert shock-compressed olivine, but not high enough to form the stable assembly of bridgmanite and wüstite. Similarly, in NWA 856, stöfflerite occurs at distances 5-20 μm away from zagamiite-stishovite assemblies (Fig. 1). Beck et al (2004) observed a similar spatial correlation in Zagami. Stöfflerite emphasizes the case of metastable formation of high-pressure minerals along a temperature gradient under dynamic stresses

because it has no stability field. Kinetic barriers permit both formation, and prevent the breakdown, of stöfflerite into the stable phases during dynamic compression. The occurrence of this minerals marks temperatures above bulk rock shock heating (by ~50-100 K around 20 - 30 GPa; Ahrens and Gregson 1964; Fritz et al. 2005), which only induces formation of diaplectic feldspatic glass (maskelynite), but below the formation of the stable phase assembly above 20 GPa, 2000 K to 22 GPa, 1500 K (Liu et al. 2012). Another constraint on the temperature of the maskelynite-stöfflerite transformation comes from the kinetic barrier of crystallization of clinopyroxene in labradorite compressed to 20 GPa, which has been interpolated to ~1000 K for 0.01s and 10% crystallization out of amorphized labradorite (Kubo et al. 2014). Formation of clinopyroxene prohibits formation of silicate-hollandites of this composition and is a first step towards formation of the stable assemblage stishovite + zagamiite. At least in shergottites, tissintite, or similar clinopyroxenes rich in the Ca-Eskola component, are observed always in the absence of (Ma et al. 2017), or in spatial separation from, stöfflerite (Beck et al. 2004). Interestingly, Kubo et al. (2014) did not observe stöfflerite as a metastable intermediate. The failure in reproducible synthesis of stöfflerite through high-pressure experiments (Liu et al. 2012; Kubo et al. 2014, 2017) points toward a combined effect of time-scale and stress rate. It is also possible that crystallization under dynamic stress follows a different sequence of metastable phase formation along the Oswald step rules as a means of reducing entropy after ramp to a super-adiabatic state on the Hugoniot line. This has been observed by Tschauner et al. (2013) for phase formations in shock-generated dense fluids.

So far, stöfflerite has been observed in shergottites and terrestrial impactites (Spray & Boonsue 2016; Boonsue & Spray 2017; Beck et al. 2004; Langenhorst & Poirier 2000), but to our knowledge not from plagioclase grains in lunar meteorites or chondrites. Clast of plagioclase

entrained in shock-melt veins of chondrites were found to decompose into lingunite and a noncrystalline calcic residue (Chen et al. 2000; El Goresy et al. 2000). The duration of the shock state in highly shocked L6-chondrites has been assessed to be much longer than in highly shocked shergottites (Sharp and deCarli 2006; Walton et al. 2014; Ma et al. 2015) but the occurrence of stöfflerite in terrestrial impactites (Spray & Boonsue 2016; Boonsue & Spray 2017), which experienced even longer shock duration, argues against time as the relevant parameter. The apparent absence of stöfflerite in chondrites and lunar meteorites may be coincidence, but it could indicate differences in the dynamic stress regime.

ACKNOWLEDGEMENTS

Part of this work was supported by DE-FG02-94ER14466, DE-NA0001974, NSF Grants EAR-1634415,-1128-799, -1322082. The Advanced Photon Source, a DOE Office of Science User Facility is operated by Argonne National Laboratory under Contract No. DE-AC02-06CH11357. The Advanced Light Source is supported through Contract No. DE-AC02-05CH11231. SEM and EPMA measurements were carried out at the Geological and Planetary Science Division Analytical Facility at Caltech, supported in part by NSF grants EAR-0318518, EAR-1322082 and DMR-0080065. OT acknowledges the support from DOE Cooperative Agreement #DE-NA0001982. JGS acknowledges support from NSERC Canada, the Canada Foundation for Innovation and the New Brunswick Innovation Foundation. We thank the reviewers Erin Walton, Martin Kunz, and Ross Angel for their helpful comments.

REFERENCES CITED

Agarwal A., Reznik, B., Kontny A., and Schilling F. (2016) Lingunite – a high-pressure plagioclase polymorph at mineral interfaces in doleritic rock in the Lockne impact structure (Sweden). Nature Scientific Reports, 6, 25991.

Ahrens, T.J., and Gregson, V.G. (1964) Shock compression of crustal rocks – data for quartz, calcite + plagioclase rocks. Journal of Geophysical Research, 69, 4839.

Akaogi,M., M. Haraguchi, M. Yaguchi, and H. Kojitani (2009) High-pressure phase relations and thermodynamic properties of CaAl4Si2O11 CAS phase, Physics of the Earth and Planetary Interiors, 173, 1–6.

Akaogi, M., M. Haraguchi, K. Nakanishi, H. Ajiro, and H. Kojitani (2010) High-pressure phase relations in the system CaAl4Si2O11-NaAl3Si3O11with implication for Na-rich CAS phase in shocked Martian meteorites, Earth and Planetary Science Letters, 289, 503–508, doi:10.1016/j.epsl.2009.11.043.

312 Beck, P., Gillet, P. Gautron, L., Daniel, I., and El Goresy, A. (2004). A new natural high-
313 pressure (Na,Ca)-hexaluminosilicate [(CaxNa1 x)Al3+xSi3 xO11] in shocked Martian
314 meteorites, Earth and Planetary Science Letters, 219, 1–12.
315 Biren, M.B., and Spray, J.G. (2011. Shock veins in the central uplift of the Manicouagan impact
316 structure: Context and genesis. Earth and Planetary Science Letters, 303, 310-322.
317 doi:10.1016/j.epsl.2011.01.003.
318 Boonsue, S., and Spray, J.G. (2017). Shock-generated labradorite polymorphs in terrestrial
319 impact rocks at Manicouagan. Lunar and Planetary Science Conference, 48, A2557.
320 Chen. M., El Goresy, A., and Gillet, P. (2000). Hollandite-type (Ca, Na)$AlSi_3O_8$ in a shock-melt
321 vein in Zagami (SNC) meteorite. European Journal of Mineralogy, 12, 30.
322 Dera, P., Zhuravlev, K., Prakapenka, V., Rivers, M.L., Finkelstein, G.J., Lavina, B., Grubor-
323 Urosevic, O., Tschauner, O., Clark, S.M., and Downs, R.T. (2013) High pressure single-
324 crystal micro X-ray diffraction analysis with GSE_ADA/RSV software. High Pressure
325 Research, 34, 1–19.
326 El Goresy A., Chen. M, Gillet, P. L., and Dubrovinski, L.S. (2000). Shock-induced high-pressure
327 phase transition of labradorite to hollandite "(Na-47-Ca-51-K-2)" in Zagami and the
328 assemblage hollandite "(Na-80-Ca-12-K-8)" plus jadeite in L chondrites: Constraints to peak
329 shock pressures. Meteoritics and Planetary Science, 35-S, A51.
330 Fritz, J., Greshake, A., and Stöffler, D. (2005) Micro-Raman spectroscopy of plagioclase and
331 maskelynite in Martian meteorites: Evidence of progressive shock metamorphism.
332 Antarctic Meteorite Research, 18, 96-116.

Gasparik, T., Tripathi, A., and Parise, J.B. (2000) Structure of a new Al-rich phase, [K, $Na]_{0.9}[Mg, Fe]_2[Mg, Fe, Al, Si]_6O_{12}$, synthesized at 24 GPa. American Mineralogist, 85, 613–618.

Gillet P., Chen M., Dubrovinsky L., and El Goresy A. 2000. Natural $NaAlSi_3O_8$-hollandite in the shocked Sixiangkou meteorite. Science, 287, 1633–1636.

Greaux, S. et al. (2018) High-pressure phase relation of KREEP basalts: A clue for finding the lost Hadean crust? Physics of the Earth and Planetary Interiors, 274, 184-194.

Huang, S., Tschauner, O., Yang, S., Humayun, M., Liu, W., Gilbert Corder, S. N., Bechtel, H. A., Tischler, J. HIMU geochemical signature originating from the transition zone. Earth and Planetary Science Letters, 542, 116323 (2020).

Kraus, W. and Nolze, G. (1996) PowderCell – a program for the representation and manipulation of crystal structures and calculation of the resulting X-ray powder patterns. Journal of Applied Crystallography, 29, 301–303.

Kubo, T. et al. (2014) Formation of a metastable hollandite phase from amorphous plagioclase. Nature Geoscience, 3, 41-45.

Kubo, T. et al. (2017) Formation of a metastable hollandite phase from amorphous plagioclase: A possible origin of lingunite in shocked chondritic meteorites. Physics of the Earth and Planetary Interiors, 272, 50-57.

Langenhorst, F. and Poirier, J.-P. (2000) 'Eclogitic' minerals in a shocked basaltic meteorite. Earth and Planetary Science Letters, 176, 259–265.

Liu, L. (1978) High-pressure phase transformations of albite, jadeite and nepheline. Earth and Planetary Science Letters, 37, 438-444.

Liu, X. et al. (2012) High-P behavior of anorthite composition and some phase relations of the CaO-Al2O3-SiO2 system to the lower mantle of the Earth, and their geophysical implications. Journal of Geophysical Research – Solid Earth, 117, Article Number: B09205.

Loewenstein, W. (1954) The distribution of aluminum in the tetrahedra of silicates and aluminates. American Mineralogist 39, 92-96.

Ma, C., Tschauner, O., Beckett, J.R., Liu, Y., Rossman, G.R., Zhuravlev, K. Prakapenka, V. B., Dera, P., Taylor, L.A. (2015) Tissintite, (Ca, Na, □)$AlSi_2O_6$, a highly-defective, shock-induced, high-pressure clinopyroxene in the Tissint martian meteorite. Earth and Planetary Science Letters, 422, 194-205.

Ma, C., Tschauner, O., Beckett, J.R., Liu, Y., Rossman, G.R., Sinogeikin, S.V., Smith, J.S., and Taylor, L.A. (2016) Ahrensite, γ-Fe_2SiO_4, a new shock-metamorphic mineral from the Tissint meteorite: Implications for the Tissint shock event on Mars. Geochimica et Cosmochimica Acta, 184, 240-256.

Ma, C., Tschauner, O., and Beckett, J.R. (2017) A new high-pressure calcium aluminosilicate ($CaAl_2Si_{3.5}O_{11}$) in martian meteorites: Another after-life for plagioclase and connections to the CAS phase. 48th Lunar and Planetary Science Conference, Abstract #1128.

Ma, C., Tschauner, O., Beckett, J.R., Rossman, G.R., Prescher, C., Prakapenke, V.B., Bechtel, H.A., and McDowell, A. (2018) Liebermannite, $KAlSi_3O_8$, a new shock-metamorphic, high-pressure mineral from the Zagami Martian meteorite. Meteoritics & Planetary Science, 53, 50-61.

Ma, C., Tschauner, O., and Beckett, J.R. (2019) A closer look at Martian meteorites: Discovery of the new mineral zagamiite, $CaAl_2Si_{3.5}O_{11}$, a shock-metamorphic, high-pressure, calcium aluminosilicate. 9th International Conference on Mars, Abstract #6138.

Madon, M., Castex, J., Peyronneaux, J. (1989) A new aluminocalcic high-pressure phase as a possible host of calcium and aluminium in the lower mantle. Nature, 342, 422 – 425, doi:10.1038/342422a0.

Pamato, M.G., Kurnosov, A., Ballaran, T.B., Trots, D.M., Caracas, R., and Frost, D.J. (2014) Hexagonal Na-0.41[Na0.125Mg0.79Al0.085](2)[Al0.79Si0.21](6)O-12 (NAL phase): Crystal structure refinement and elasticity. American Mineralogist, 99, 1562-1569.

Post, J.E. and Burnham, C.W. (1986) Modelling tunnel-cation displacements in hollandites using structure-energy calculations. American Mineralogist 71, 1178- 1185.

Prescher, C., and Prakapenka, V.B. (2015) DIOPTAS : a program for reduction of two-dimensional X-ray diffraction data and data exploration. High Pressure Research, 35, 223–230.

Putz, H., J.C. Schön, J.C., and Jansen, M. (1999) Combined method for *ab initio* structure solution from powder diffraction data. Journal of Applied Crystallography, 32, 864–870.

Ringwood, A. E., Reid, A. F., and Wadsley, A. D. (1967) High-pressure $KAlSi_3O_8$: An aluminosilicate with six-fold coordination: Acta Crystallographica, 23, 1093–1095.

Sharp T.G. and DeCarli, P.S. (2006). Shock effects in meteorites, in: Meteorites and the Early Solar System II, 653- 677. Publisher: University of Arizona Press, Tucson.

Smith, D.G.W., and Nickel, E.H. (2007) A system for codification for unnamed minerals: report of the Subcommittee for Unnamed Minerals of the IMA Commission on New Minerals, Nomenclature and Classification. Canadian Mineralogist, 45, 983−1055.

Spray, J.G., Boonsue, S. (2016) Monoclinic and tetragonal plagioclase (An_{54}) in shock veins from the central uplift of the Manicouagan impact structure. Meteoritics and Planetary Science Conference 51-S1, A6117.

Stöffler, D, Hamann, C., and Metzler, K. (2018) Shock metamorphism of planetary silicate rocks and sediments: Proposal for an updated classification system. Meteoritics & Planetary Science, 53, 5-49.

Tomioka, N., Mori, H., and Fujino K. (2000) Shock-induced transition of $NaAlSi_3O_8$ feldspar into a hollandite structure in a L6 chondrite. Geophysical Research Letters 27, 3997–4000.

Tschauner, O., Luo, S.N., Chen, Y.J., McDowell, A., Knight, J., and Clark, S.M. (2013) Shock synthesis of Lanthanum-III-pernitride. High Pressure Research Volume 33, Issue 1, 202-206.

Tschauner, O., Ma, C., Beckett, J., Prescher, C., Prakapenka, V.B., Rossman, G.R. (2014) Discovery of Bridgmanite – the most abundant mineral in Earth, in a shocked meteorite. Science 346, 1100 – 1102.

Tschauner, O. and Ma, C. (2017) Stöfflerite, IMA 2017-062. CNMNC Newsletter No. 39, October 2017, page 1285; Mineralogical Magazine, 81, 1279–1286.

Von Dreele, R. B., and Larson, A. C. (2004) General Structure Analysis System (GSAS) Los Alamos National Laboratory Report LAUR, New Mexico

Walton, E.L., Sharp, T.G., Hu, J., Filiberto, J., 2014. Heterogeneous mineral assemblages in martian meteorite Tissint as a result of a recent small impact event on Mars. Geochimica et Cosmochimica Acta, 140, 334-348.

Xie X., Chen M., Wang D., and El Goresy A. (2001) $NaAlSi_3O_8$-hollandite and other high-pressure minerals in the shock melt veins of the Suizhou meteorite. Chinese Science Bulletin, 46, 1116-1125.

Zel'dovich, Y.B. & Raizer, Y.P. Physics of Shock Waves and High-Temperature Hydrodynamic Phenomena. Section V, Cambridge University Press 2002,

Zhang, J, Ko, J, Hazen, R.M., and Prewitt, C.T. (1993) High-pressure crystal chemistry of KAlSi3O8 hollandite. American Mineralogist, 78, 493-499.

This is the peer-reviewed, final accepted version for American Mineralogist, published by the Mineralogical Society of America.
The published version is subject to change. Cite as Authors (Year) Title. American Mineralogist, in press.
DOI: https://doi.org/10.2138/am-2021-7563. http://www.minsocam.org/

427

428 Table 1. Mean electron microprobe (WDS) analytical data (n=11) for stöfflerite in NWA 856.

429 All Fe in the ferric state.

Oxide	wt%	Range	SD	Detection Limit	Probe Standard	Formula unit (8 oxygens)
SiO_2	55.47	55.26-57.69	0.83	0.03	Anorthite	2.49
TiO_2	0.06	0.00-0.23	0.08	0.07	Rutile	0.00
Al_2O_3	28.25	27.45-28.46	0.40	0.02	Anorthite	1.49
Cr_2O_3	0.04	0.00-0.15	0.05	0.10	Cr_2O_3	0.00
Fe_2O_3	0.83	0.62-0.96	0.11	0.15	Fayalite	0.03
MnO	0.04	0.00-0.18	0.05	0.11	Mn_2SiO_4	0.00
MgO	0.07	0.03-0.40	0.11	0.02	Forsterite	0.00
CaO	11.46	9.57-11.59	0.76	0.03	Anorthite	0.55
Na_2O	4.19	3.24-4.42	0.40	0.03	Albite	0.36
K_2O	0.27	0.25-0.37	0.04	0.02	Microcline	0.02
Total	100.69					12.95

430

This is the peer-reviewed, final accepted version for American Mineralogist, published by the Mineralogical Society of America.
The published version is subject to change. Cite as Authors (Year) Title. American Mineralogist, in press.
DOI: https://doi.org/10.2138/am-2021-7563. http://www.minsocam.org/

431

432

433

434

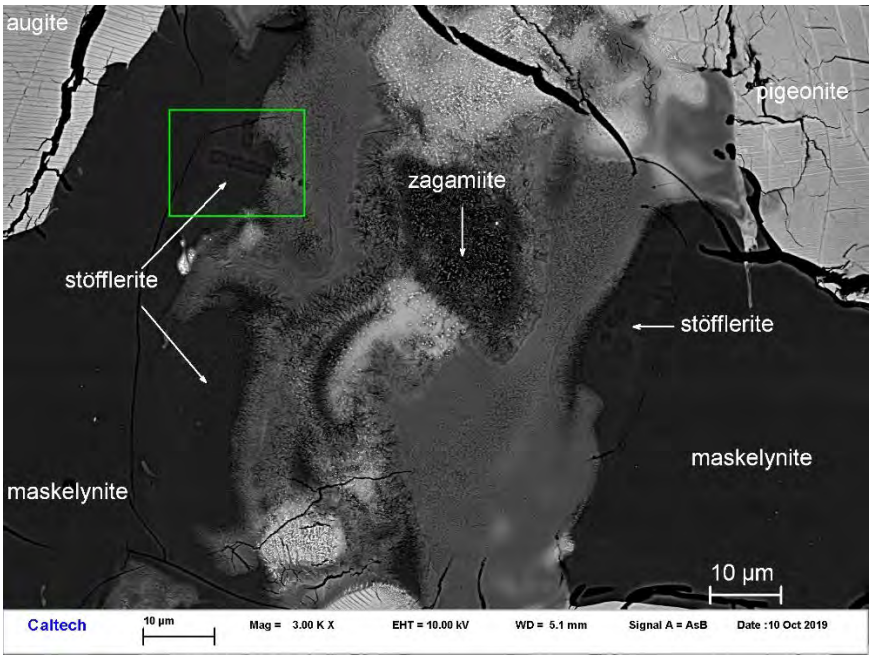

435

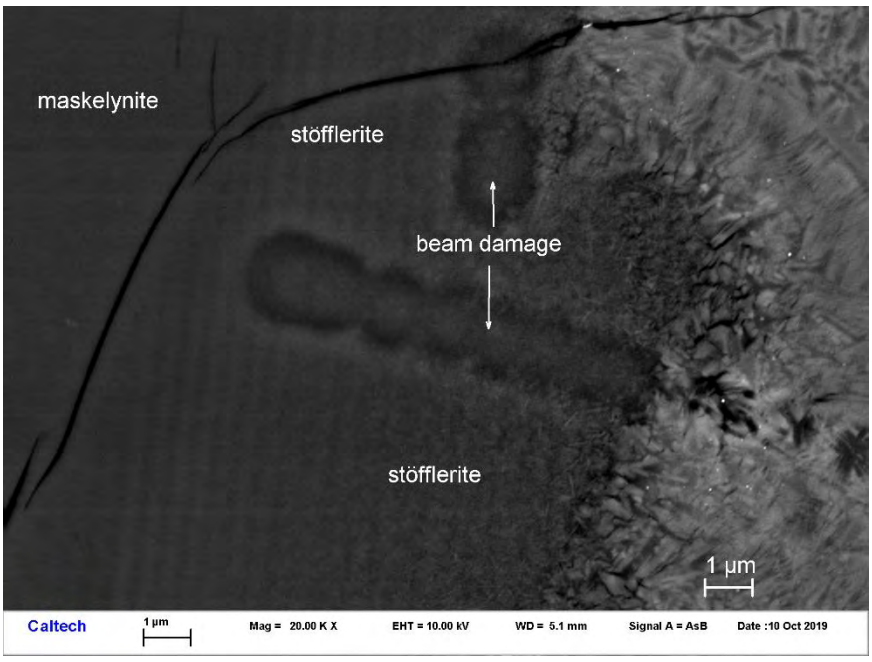

436

437 Figure 1. BSE images showing stöfflerite in contact with a shock melt pocket in NWA 856.

438 Stöfflerite is electron-beam sensitive. The dots in the stöfflerite region were due to beam

439 damage.

440

441

442

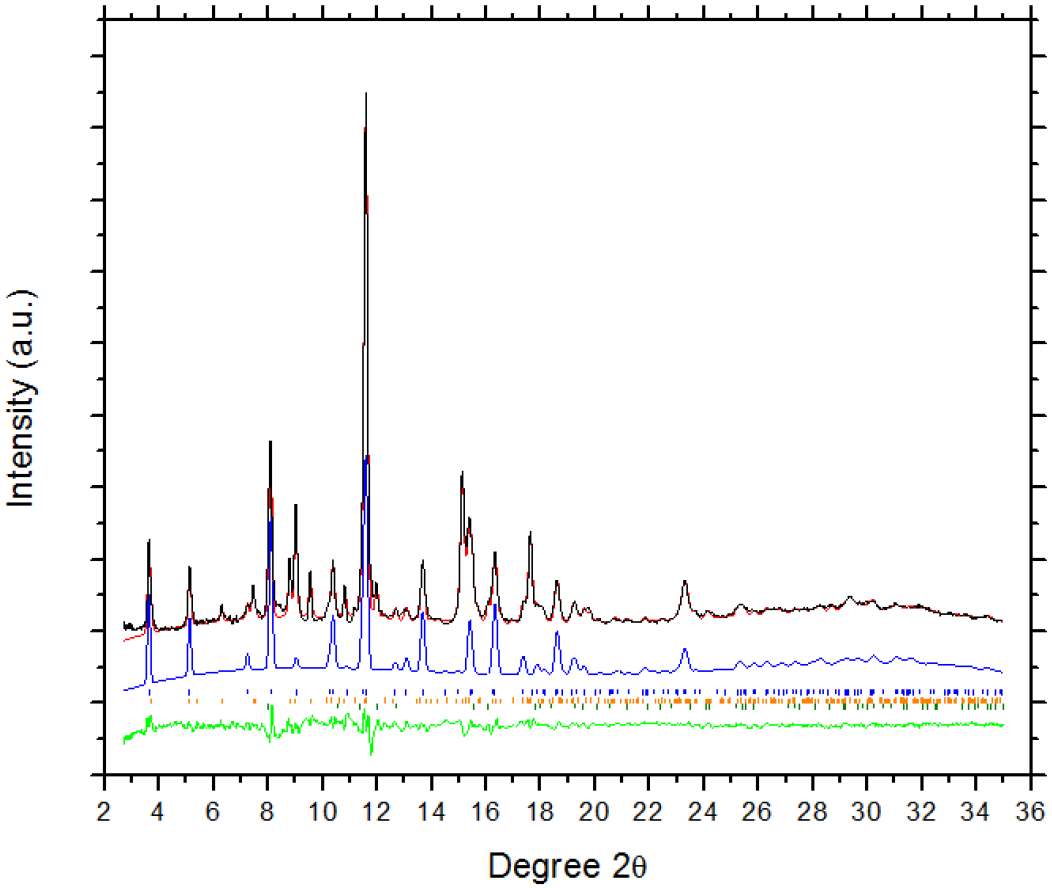

443

444 Figure 2. Representative X-ray diffraction pattern (black) of the stöfflerite type material in NWA
445 856 (Stöfflerite52Lingunite45Liebermannite3). Modeled pattern from Rietveld refinement (red):
446 stöfflerite (80 -85 vol%), zagamiite (12-15%), and stishovite (5 - 8%). The modeled, refined
447 pattern of stöfflerite only is shown in blue (with constant offset for better visualization). The
448 residual of fit is shown in green. Blue, orange, and dark green tickmarks represent observable
449 reflections of stöfflerite, zagamiite, and stishovite, respectively. The primary beam wavelength
450 was 0.4133 Å.

This is the peer-reviewed, final accepted version for American Mineralogist, published by the Mineralogical Society of America.
The published version is subject to change. Cite as Authors (Year) Title. American Mineralogist, in press.
DOI: https://doi.org/10.2138/am-2021-7563. http://www.minsocam.org/

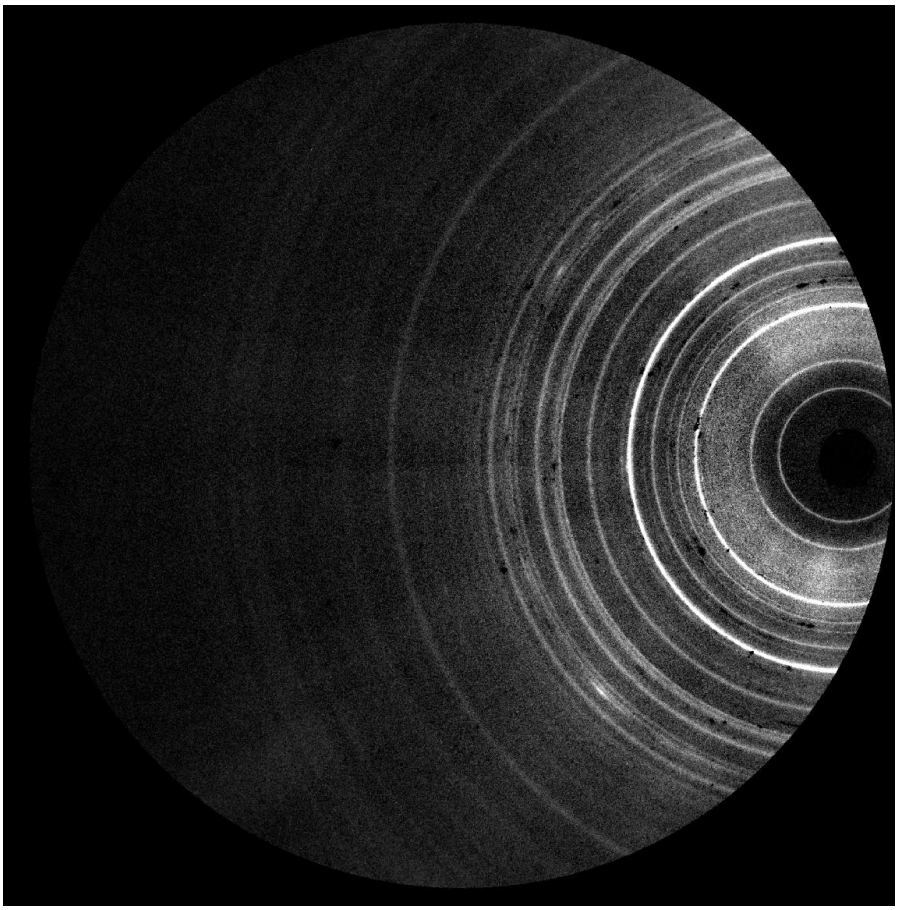

Figure 2b: Diffraction image frame corresponding to Figure 2a. A pattern of maskelynite from the same thin section of NWA 856 was used as brackground frame (same as for the integrated pattern in Figure 2a). A few dark spots are from pyroxene inclusions in the brackground frame.